H1prelim-19-032

Quantum entanglement of partons in the proton and a new measurement of charged particle multiplicity distributions in deep-inelastic scattering at HERA

H1 Collaboration

Abstract

New experimental data on charged particle multiplicity distributions are presented, covering the kinematic ranges in momentum transfer $5 < Q^2 < 100$ GeV^2 and inelasticity $0.0375 < y < 0.6$. The data were recorded with the H1 experiment at the HERA collider in positron-proton collisions at a centre-of-mass energy of 320 GeV. Charged particles are counted with transverse momenta $P_T > 150$ MeV and pseudorapidity $-1.6 < \eta_{\rm lab} < 1.6$ in the laboratory frame, corresponding to high acceptance in the current hemisphere of the hadronic centre-of-mass frame. Charged particle multiplicities are reported on a two-dimensional grid of Q^2, y and on a three-dimensional grid of Q^2, y, η. The observable is the probability $P(N)$ to observe N particles in the given η region. The data are confronted with predictions from Monte Carlo generators, and with a simplistic model based on quantum entanglement and strict parton-hadron duality.

1 Introduction

In the parton model [1–3] formulated by Bjorken, Feymann, and Gribov, the bounded quarks and gluons of a nucleon are viewed as "quasi-free" particles by an external hard probe in the infinite momentum frame. The parton that participates in the hard interaction with the probe, e.g., the virtual photon, is expected to be causally disconnected from the rest of the nucleon. On the other hand, the parton and the rest of the nucleon have to form a colour-singlet state due to colour confinement. In order to further understand the role of colour confinement in high energy collisions, it has been suggested [4, 5] that the quantum entanglement of partons could be an important probe to the underlying mechanism of confinement.

In recent years, the idea of considering quantum entanglement in high energy collisions have been realized and many interesting results have been found both theoretically [5–8] and experimentally [9, 10]. For example, in a study by Tu et al [10] based on data at the Large Hadron Collider (LHC), the entropy of charged particles produced in proton-proton (pp) collisions is found to have a strong correlation to the entanglement entropy predicted by the gluon density [5], which shows a first indication of quantum entanglement of partons inside of proton. However, in high energy pp collisions, there are other phenomena that might play an important role in particle productions, e.g., Multiple Parton Interaction (MPI), Colour Reconnection (CR), and etc. Therefore, the entanglement of partons can be investigated in electron-proton (ep) deep inelastic scattering (DIS) events with better-defined theoretical interpretations.

In high energy ep DIS process, the hard interaction between the virtual photon and the parton defines a transverse spatial domain by a size of $1/Q$ within the target proton, where Q is defined by the virtuality of the photon. The collision separates the target proton into a probed region and a proton remnant, denoted by region A and B, respectively. In the parton model where the collinear factorization is assumed, region A and B are expected to be causally disconnected and therefore have no correlation. However, if partons in region A and B are entangled quantum mechanically, the entanglement entropy of A and B would be identical, e.g., $S_{\mathrm{A}} = S_{\mathrm{B}}$. Based on Refs. [5, 10], the entanglement entropy in DIS was found to have a simple relation with the gluon density $xG(x, Q^2)$ in the low-x limit as, $S_{\mathrm{parton}} = \ln[xG(x)]$[1]. This was inspired by a well known result for the entanglement entropy in $(1+1)$ conformal field theory [5, 11–13], where the length of the studied region in the context of DIS is $(1/mx)$[2] which is closely related to parton distributions. In addition, it is suggested [5] that the proportionality is expected to be valid between the final-state hadron entropy, S_{hadron}, and the initial-state parton entropy, S_{parton}, due to the "parton liberation" [14] and "local parton-hadron duality (LPHD)" [15] pictures. Therefore, the entanglement entropy S_{A} (equivalent to notation S_{EE}) can be revealed by the final-state hadron entropy, e.g.,

$$S_{\mathrm{parton}} = \ln[xG(x)] = S_{\mathrm{hadron}} = -\sum P(N) \ln P(N). \tag{1}$$

where $P(N)$ is the charged particle multiplicity distribution.

Similar multiplicity measurements have been done at HERA and at the LHC [16–25]. However these measurements in ep DIS were not precise towards the high multiplicity tail nor in

[1] Hereafter the Q^2 dependence of gluon density is dropped for simplicity, denoted as $xG(x)$

[2] In the target rest frame, m is the proton rest mass, $(1/mx) \sim (1/x)$

the form of double-differential bins in x and Q^2 in order to be mapped to the parton distribution function, which are both important in testing quantum entanglement proposed by Ref [10]. Thus, measuring multiplicity distributions in ep DIS with more statistics in kinematic bins of x and Q^2 are strongly motivated. The relation in Eq. 1 can be explicitly verified using the ep DIS data within measurable phase spaces.

Despite the new idea of relating final-state hadron multiplicity to the entanglement entropy of partons, charged particle production has been extensively studied in high energy collisions over many decades, from electron-positron (e^+e^-) scattering to heavy ion collisions. For reviews, see Refs. [26–29] and the references therein. On the one hand, the exact particle production mechanism and quantitative prediction of multiplicity distributions are not yet completely understood in hadron (nucleus) collider experiments due to the complicated substructure of nucleon and parton fragmentation. For example, no first-principle calculation can describe the multiplicity distributions at the LHC in pp collisions, and no phenomenology model can reproduce those distributions without significant tuning [30]. On the other hand, the measurement of entanglement entropy of partons via final-state hadron might provide a new perspective to particle productions without directly considering fragmentation. For instance, the entanglement entropy in high energy collisions implies a natural upper limit on the particle multiplicity density [5], similar to the prediction from the theory of Color Glass Condense with gluon saturation [31].

2 Result

2.1 Multiplicity distributions

The charged particle multiplicity distributions in ep DIS at $\sqrt{s} = 319\,\text{GeV}$ are measured between $|\eta_{\text{lab}}| < 1.6$ in the lab frame, shown in Fig. 1. Different Q^2 and y bins are shown in different panels, where the Q^2 ranges between 5 to 100 GeV^2 and y is between 0.0375 to 0.6. The $P(N)$ distributions are fully unfolded, where the statistical uncertainty is denoted by the error bar and the systematic uncertainty is represented by the shaded box. The data are compared with generated truth level of the MC generators of DJANGOH, RAPGAP, and PYTHIA 8.

From Fig. 2 to Fig. 5, the charged particle multiplicity distributions $P(N)$ in Q^2 bins $(5, 10)$, $(10, 20)$, $(20, 40)$, and $(40, 100)$ GeV^2 are presented, respectively. In each figure, the $P(N)$ distributions are shown differentially in bins of y (identical binning as in Fig. 1), and in bins of η_{lab}. The η_{lab} bins are presented between $-1.2 < \eta_{\text{lab}} < 0.2$, $-0.5 < \eta_{\text{lab}} < 0.9$, and $0.2 < \eta_{\text{lab}} < 1.6$ in the lab frame.

In Fig. 6, the multiplicity distributions, $P(N)$, is measured in the pseudorapidity range $0 < \eta^* < 4.0$ in the HCM frame. To minimize the extrapolation in multiplicity, an additional requirement of $|\eta_{\text{lab}}| < 1.6$ and $p_{\text{T,lab}} > 150$ MeV/c in the lab frame is imposed. This requirement is the same for all HCM measurements hereafter. The predictions of DJANGOH, RAPGAP, and PYTHIA 8 are compared with data, shown as dotted lines. Similar dependences on y and Q^2 are found, similar to the results measured in the lab frame. The MC descriptions of data are generally better in the HCM frame than in the lab frame, where the RAPGAP generator is found to have the best agreement with the data among all presented MC models.

In order to further study the multiplicity distribution, the KNO function $\Psi(z)$ is measured as a function $z = N/\langle N\rangle$ in different Q^2 bins, shown in Fig. 7. Different data points correspond to different bins in W (or $\langle y\rangle$) in the HCM frame between $0 < \eta^* < 4$. KNO scaling has been observed over the measured Q^2 and W range. Similar measurements were done both at PETRA and HERA experiments at DESY and Large Electron Positron (LEP) experiments [20, 21, 32–34], where a similar conclusion that the KNO scaling was observed as to the current measurement.

2.2 Moments of multiplicity distributions

In Fig. 8, the mean multiplicity $\langle N_{\mathrm{ch}}\rangle$ as a function of W using particles with transverse momentum $p_{\mathrm{T,lab}} > 150\ \mathrm{MeV/c}$ within pseudorapidity range $|\eta_{\mathrm{lab}}| < 1.6$ in the lab frame (left) and $0 < \eta^* < 4.0$ in the HCM frame (right), are shown. The corresponding $\langle y\rangle$ value in each bin are drawn on the top axis of each figure. The prediction obtained with the MC event generator RAPGAP is compared with data denoted by the lines. Other MC models have been compared and generally with poorer description of the data than with RAPGAP, thus not shown.

Similarly, in Fig. 9, second moments of multiplicity distributions, the variance, are shown as a function of W using particles with transverse momentum $p_{\mathrm{T,lab}} > 150\ \mathrm{MeV/c}$ within pseudorapidity range $|\eta_{\mathrm{lab}}| < 1.6$ in the lab frame (left) and $0 < \eta^* < 4.0$ in the HCM frame (right). All measured Q^2 bins are presented and indicated in the legend.

2.3 Entropy

It is recently suggested by Refs. [5,10] that the Boltzmann entropy of final-state particles can be calculated based on the charged particle multiplicity distributions, which might indicate a deep connection to the entanglement entropy of gluons at low-x. In Fig. 10, the Boltzmann entropy of final-state hadron, S_{hadron}, is studied as a function of $\langle x\rangle$ in different Q^2 bins. The total uncertainty is indicated by the error bar, where the statistical and systematic uncertainty are added in quadrature. For each different $\langle x\rangle$ (or y) bin, the selected pseudorapidity window in the lab frame is used for measuring the multiplicity, e.g., $-1.2 < \eta_{\mathrm{lab}} < 0.2$ at $\langle x\rangle \sim 3\times10^{-4}$, $-0.5 < \eta_{\mathrm{lab}} < 0.9$ at $\langle x\rangle \sim 7\times10^{-4}$, and $-0.2 < \eta_{\mathrm{lab}} < 1.6$ at $\langle x\rangle \sim 1.3\times10^{-3}$. Similar to the observable studied in Ref. [10], the varying η_{lab} range is intended for matching the rapidity of the scattered quark from the DIS process in a leading order picture, which is closely related to the region A introduced earlier. The same observable is studied using MC event generator RAPGAP, which qualitatively agrees with the data at each measured Q^2 bin. On the other hand, the predictions from entanglement entropy based on the gluon density $xG(x)$ are also shown for comparison at various of Q^2 values, indicated by the open markers with coloured bands. The couloured bands indicate the systematic uncertainty suggested as given by the parton density at the 95% confidence level. The Parton Distribution Function (PDF) set is HERAPDF 2.0 at the leading order.

Taking one step further, it is possible to measure the Boltzmann entropy of particles from the current fragmentation hemisphere with 4 units of pseudorapidity coverage, shown in Fig. 11. Unfortunately, only very limited access to the target fragmentation region is possible in H1 experiment, and therefore, not presented. In Fig. 11, the hadron entropy based on multiplicity distributions are studied as a function of $\langle x \rangle$ in different Q^2 bins within a fixed pseudorapidity range $0 < \eta^* < 4.0$ in the HCM frame. The MC model RAPGAP are shown with lines, where the predictions from entanglement entropy based on gluon densities are shown in open markers with coloured bands, identical to that in Fig. 10.

3 Summary

The charged particle multiplicity distributions, $P(N)$, in deep inelastic scattering events at $\sqrt{s} = 319\,\text{GeV}$ using the H1 detector at HERA are measured. The total integrated luminosity used in this analysis is around $136\ \text{pb}^{-1}$, recorded by the H1 detector between 2006 and 2007 in positions scattering off protons. The $P(N)$ distributions are measured in bins of Q^2 , y, and pseudorapidity η, both in the lab and the HCM frames. The results are generally found to be consistent with Monte Carlo (MC) event generators at low multiplicity, while they are significantly different at the high multiplicity tail in all measured kinematic bins. Furthermore, the MC generators tend to describe better the high Q^2 and low y events, while poorly for low Q^2 and high y events. This is a strong indication of underestimating important physics process and contributions at high multiplicity, low-x, and low-Q^2 regions, in the event generator. The Boltzmann entropy based on multiplicity distributions are found to be not consistent with the prediction from entanglement entropy of gluons, while further theoretical calculations of entanglement entropy with Q^2 evolution including sea partons is needed for a proper comparison to the measured data.

Acknowledgements

We are grateful to the HERA machine group whose outstanding efforts have made this experiment possible. We thank the engineers and technicians for their work in constructing and maintaining the H1 detector, our funding agencies for financial support, the DESY technical staff for continual assistance and the DESY directorate for support and for the hospitality which they extend to the non–DESY members of the collaboration.

We would like to give credit to all partners contributing to the EGI computing infrastructure for their support for the H1 Collaboration.

We express our thanks to all those involved in securing not only the H1 data but also the software and working environment for long term use, allowing the unique H1 data set to continue to be explored in the coming years. The transfer from experiment specific to central resources with long term support, including both storage and batch systems, has also been crucial to this enterprise. We therefore also acknowledge the role played by DESY-IT and all people involved during this transition and their future role in the years to come.

References

[1] J. D. Bjorken and E. A. Paschos, Inelastic Electron Proton and gamma Proton Scattering, and the Structure of the Nucleon, Phys. Rev. **185**, 1975 (1969).

[2] R. P. Feynman, The behavior of hadron collisions at extreme energies, Conf. Proc. **C690905**, 237 (1969).

[3] V. N. Gribov, A reggeon diagram technique, Sov. Phys. JETP **26**, 414 (1968), [Zh. Eksp. Teor. Fiz.53,654(1967)].

[4] I. R. Klebanov, D. Kutasov, and A. Murugan, Entanglement as a probe of confinement, Nucl. Phys. **B796**, 274 (2008), 0709.2140.

[5] D. E. Kharzeev and E. M. Levin, Deep inelastic scattering as a probe of entanglement, Phys. Rev. **D95**, 114008 (2017), 1702.03489.

[6] H. Duan, C. Akkaya, A. Kovner, and V. V. Skokov, Entanglement or ignorance: which is responsible for parton model? (2020), 2001.01726.

[7] N. Armesto, F. Dominguez, A. Kovner, M. Lublinsky, and V. Skokov, The Color Glass Condensate density matrix: Lindblad evolution, entanglement entropy and Wigner functional, JHEP **05**, 025 (2019), 1901.08080.

[8] A. Kovner and M. Lublinsky, Entanglement entropy and entropy production in the Color Glass Condensate framework, Phys. Rev. **D92**, 034016 (2015), 1506.05394.

[9] O. K. Baker and D. E. Kharzeev, Thermal radiation and entanglement in proton-proton collisions at energies available at the CERN Large Hadron Collider, Phys. Rev. **D98**, 054007 (2018), 1712.04558.

[10] Z. Tu, D. E. Kharzeev, and T. Ullrich, The EPR paradox and quantum entanglement at sub-nucleonic scales (2019), 1904.11974.

[11] R. Peschanski, Dynamical entropy of dense QCD states, Phys. Rev. **D87**, 034042 (2013), 1211.6911.

[12] R. Peschanski and S. Seki, Entanglement Entropy of Scattering Particles, Phys. Lett. **B758**, 89 (2016), 1602.00720.

[13] V. Balasubramanian, M. B. McDermott, and M. Van Raamsdonk, Momentum-space entanglement and renormalization in quantum field theory, Phys. Rev. **D86**, 045014 (2012), 1108.3568.

[14] A. H. Mueller, Toward equilibration in the early stages after a high-energy heavy ion collision, Nucl. Phys. **B572**, 227 (2000), hep-ph/9906322.

[15] Y. L. Dokshitzer, V. A. Khoze, and S. I. Troyan, On the concept of local parton-hadron duality, Journal of Physics G: Nuclear and Particle Physics **17**, 1585 (1991).

[16] G. Aad *et al.*, Charged-particle distributions in pp interactions at $\sqrt{s} = 8$ TeV measured with the ATLAS detector, Eur. Phys. J. **C76**, 403 (2016), 1603.02439.

[17] S. Acharya *et al.*, Charged-particle multiplicity distributions over a wide pseudorapidity range in proton-proton collisions at $\sqrt{s} =$ 0.9, 7, and 8 TeV, Eur. Phys. J. **C77**, 852 (2017), 1708.01435.

[18] V. Khachatryan *et al.*, Charged particle multiplicities in pp interactions at $\sqrt{s} = 0.9$, 2.36, and 7 TeV, JHEP **01**, 079 (2011), 1011.5531.

[19] R. Aaij *et al.*, Measurement of charged particle multiplicities and densities in pp collisions at $\sqrt{s} = 7$ TeV in the forward region, Eur. Phys. J. **C74**, 2888 (2014), 1402.4430.

[20] S. Chekanov *et al.*, Energy dependence of the charged multiplicity in deep inelastic scattering at HERA, JHEP **06**, 061 (2008), 0803.3878.

[21] C. Adloff *et al.*, Evolution of e p fragmentation and multiplicity distributions in the Breit frame, Nucl. Phys. B **504**, 3 (1997), hep-ex/9707005.

[22] S. Aid *et al.*, Charged particle multiplicities in deep inelastic scattering at HERA, Z. Phys. **C72**, 573 (1996), hep-ex/9608011.

[23] F. D. Aaron *et al.*, Observation of the Hadronic Final State Charge Asymmetry in High Q**2 Deep-Inelastic Scattering at HERA, Phys. Lett. B **681**, 125 (2009), 0907.2666.

[24] F. D. Aaron *et al.*, Charged Particle Production in High Q**2 Deep-Inelastic Scattering at HERA, Phys. Lett. B **654**, 148 (2007), 0706.2456.

[25] C. Adloff *et al.*, Multiplicity structure of the hadronic final state in diffractive deep inelastic scattering at HERA, Eur. Phys. J. C **5**, 439 (1998), hep-ex/9804012.

[26] F. Becattini, A thermodynamical approach to hadron production in ee collisions, Zeitschrift für Physik C Particles and Fields **69**, 485 (1995).

[27] L. V. Hove, Particle production in high energy hadron collisions, Physics Reports **1**, 347 (1971).

[28] G. Giacomelli, Particle production in high energy collisions (2009), 0901.4924.

[29] X.-N. Wang, Particle production in high-energy heavy ion collisions, in *Multiparticle dynamics. Proceedings, 31st International Symposium, ISMD 2001, Datong, China, September 1-7, 2001* (2001), pp. 170–183, hep-ph/0111404.

[30] R. Corke and T. Sjostrand, Interleaved Parton Showers and Tuning Prospects, JHEP **03**, 032 (2011), 1011.1759.

[31] F. Gelis, E. Iancu, J. Jalilian-Marian, and R. Venugopalan, The Color Glass Condensate, Ann. Rev. Nucl. Part. Sci. **60**, 463 (2010), 1002.0333.

[32] W. Braunschweig *et al.*, Charged Multiplicity Distributions and Correlations in e+ e- Annihilation at PETRA Energies, Z. Phys. **C45**, 193 (1989).

[33] P. Abreu *et al.*, Charged particle multiplicity distributions in Z0 hadronic decays, Z. Phys. **C50**, 185 (1991).

[34] D. Decamp *et al.*, Measurement of the charged particle multiplicity distribution in hadronic Z decays, Phys. Lett. **B273**, 181 (1991).

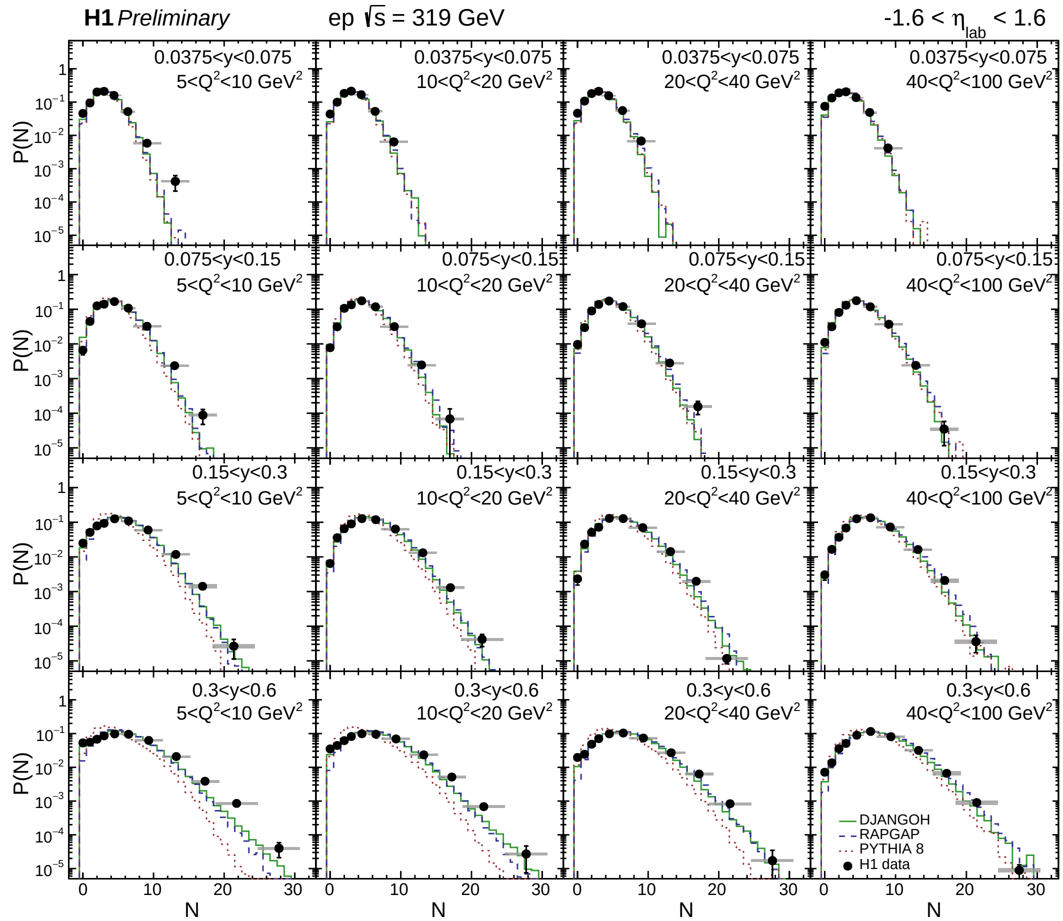

Figure 1: The charged particle multiplicity distributions, $P(N)$, are shown as a function of N particles at $\sqrt{s} = 319\,\text{GeV}$ ep collisions for particles within pseudorapidity range $|\eta_{\rm lab}| < 1.6$. Different panels correspond to different Q^2 and y bins, indicated by the legends in the figure. The MC particle level multiplicity distributions from DJANGOH, RAPGAP, and PYTHIA 8, are also shown for comparison. The statistical uncertainty is denoted by the error bars. The systematic uncertainty is shown with the shaded box. For intervals wider than one unit in multiplicity, the quantity $P(N)/\Delta N$ is shown. Along the horizontal axis, the data are drawn at the geometrical bin center.

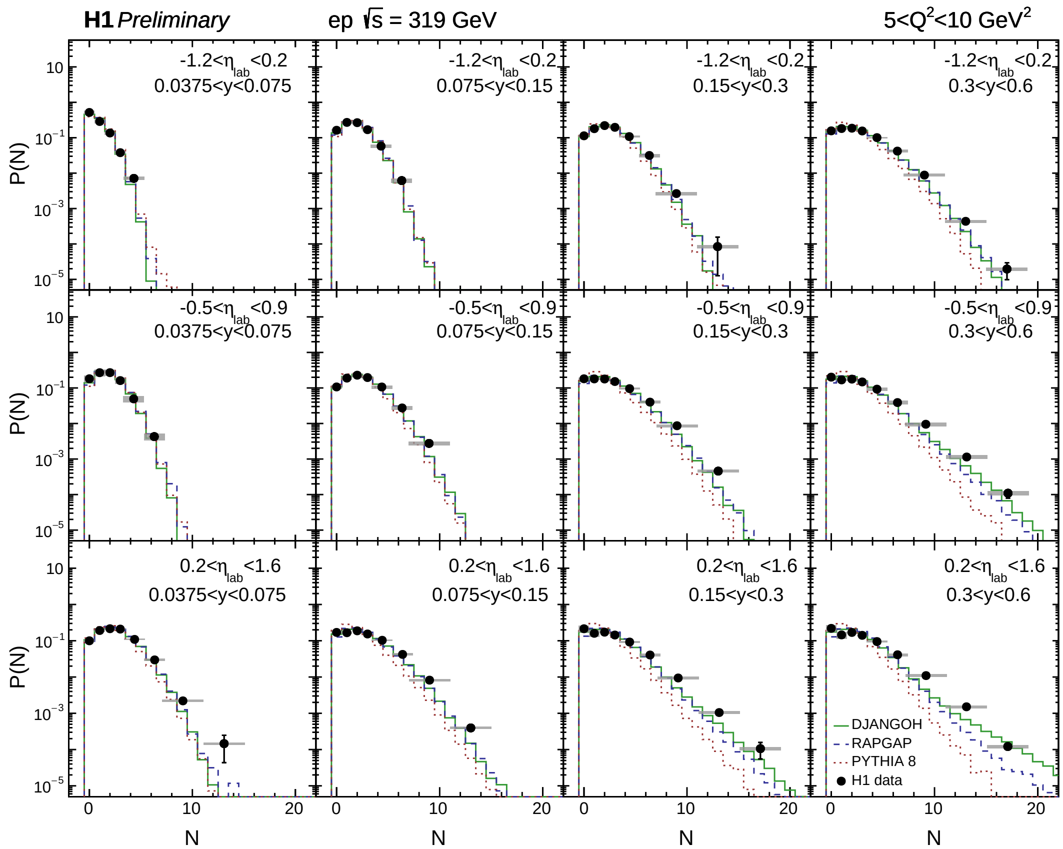

Figure 2: The charged particle multiplicity distributions, $P(N)$, are shown as a function of N particles at $\sqrt{s} = 319\,\mathrm{GeV}$ ep collisions for events with $5 < Q^2 < 10\ \mathrm{GeV}^2$. Different panels correspond to different η_{lab} and y bins, indicated by the legends in the figure. The MC particle level multiplicity distributions from DJANGOH, RAPGAP, and PYTHIA 8, are also shown for comparison. The statistical uncertainty is denoted by the error bars. The systematic uncertainty is shown with the shaded box. For intervals wider than one unit in multiplicity, the quantity $P(N)/\Delta N$ is shown. Along the horizontal axis, the data are drawn at the geometrical bin center.

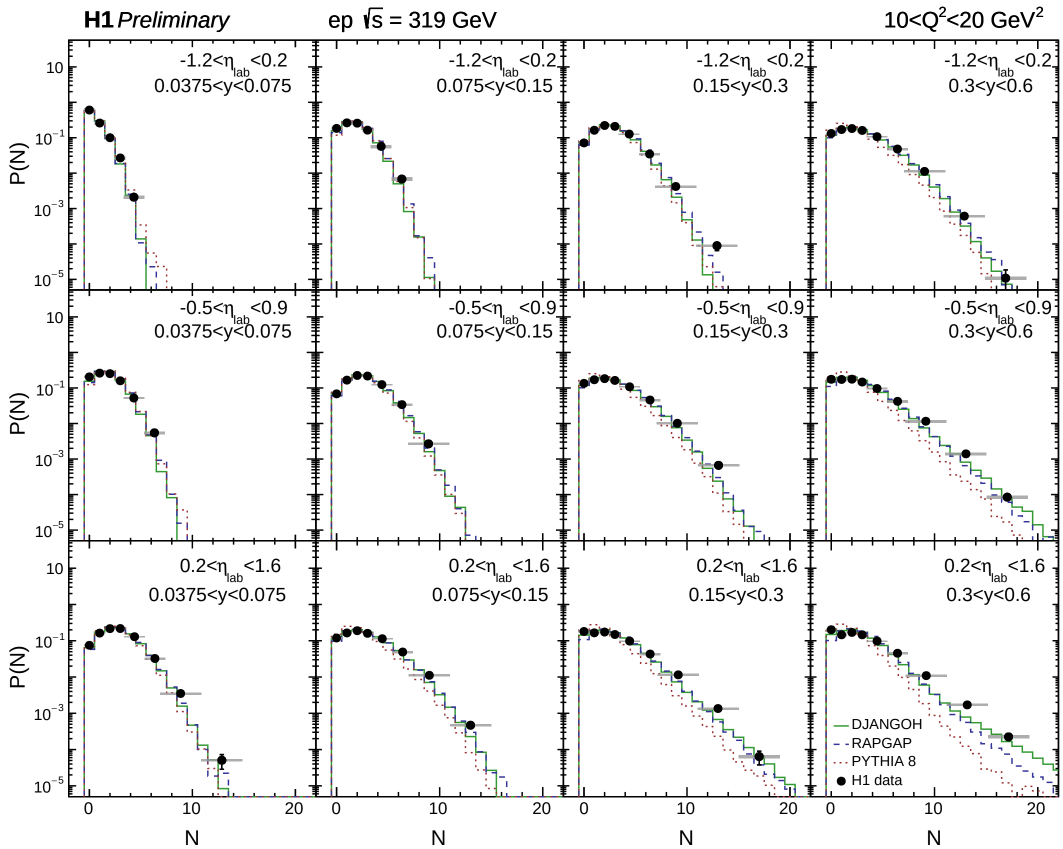

Figure 3: The charged particle multiplicity distributions, $P(N)$, are shown as a function of N particles at $\sqrt{s} = 319\,\text{GeV}$ ep collisions for events with $10 < Q^2 < 20\ \text{GeV}^2$. Different panels correspond to different η_{lab} and y bins, indicated by the legends in the figure. The MC particle level multiplicity distributions from DJANGOH, RAPGAP, and PYTHIA 8, are also shown for comparison. The statistical uncertainty is denoted by the error bars. The systematic uncertainty is shown with the shaded box. For intervals wider than one unit in multiplicity, the quantity $P(N)/\Delta N$ is shown. Along the horizontal axis, the data are drawn at the geometrical bin center.

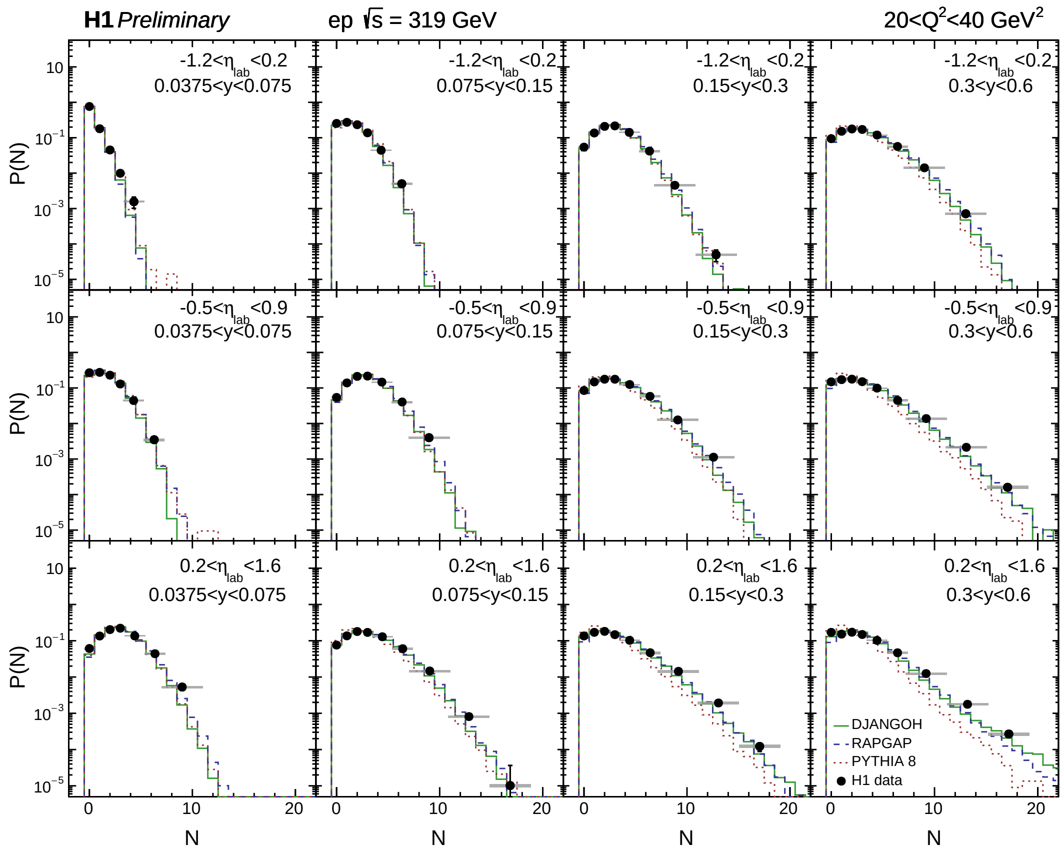

Figure 4: The charged particle multiplicity distributions, $P(N)$, are shown as a function of N particles at $\sqrt{s} = 319\,\mathrm{GeV}$ ep collisions for events with $20 < Q^2 < 40\ \mathrm{GeV}^2$. Different panels correspond to different η_{lab} and y bins, indicated by the legends in the figure. The MC particle level multiplicity distributions from DJANGOH, RAPGAP, and PYTHIA 8, are also shown for comparison. The statistical uncertainty is denoted by the error bars. The systematic uncertainty is shown with the shaded box. For intervals wider than one unit in multiplicity, the quantity $P(N)/\Delta N$ is shown. Along the horizontal axis, the data are drawn at the geometrical bin center.

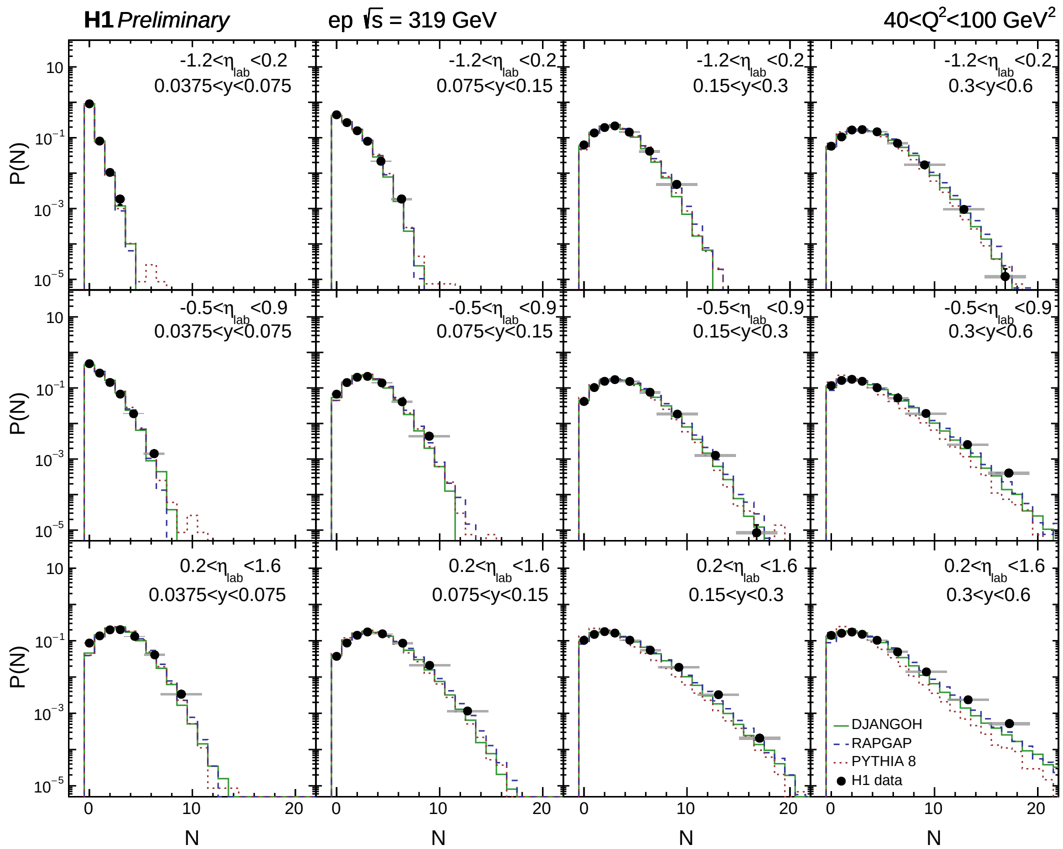

Figure 5: The charged particle multiplicity distributions, $P(N)$, are shown as a function of N particles at $\sqrt{s} = 319\,\mathrm{GeV}$ ep collisions for events with $40 < Q^2 < 100\ \mathrm{GeV}^2$. Different panels correspond to different η_{lab} and y bins, indicated by the legends in the figure. The MC particle level multiplicity distributions from DJANGOH, RAPGAP, and PYTHIA 8, are also shown for comparison. The statistical uncertainty is denoted by the error bars. The systematic uncertainty is shown with the shaded box. For intervals wider than one unit in multiplicity, the quantity $P(N)/\Delta N$ is shown. Along the horizontal axis, the data are drawn at the geometrical bin center.

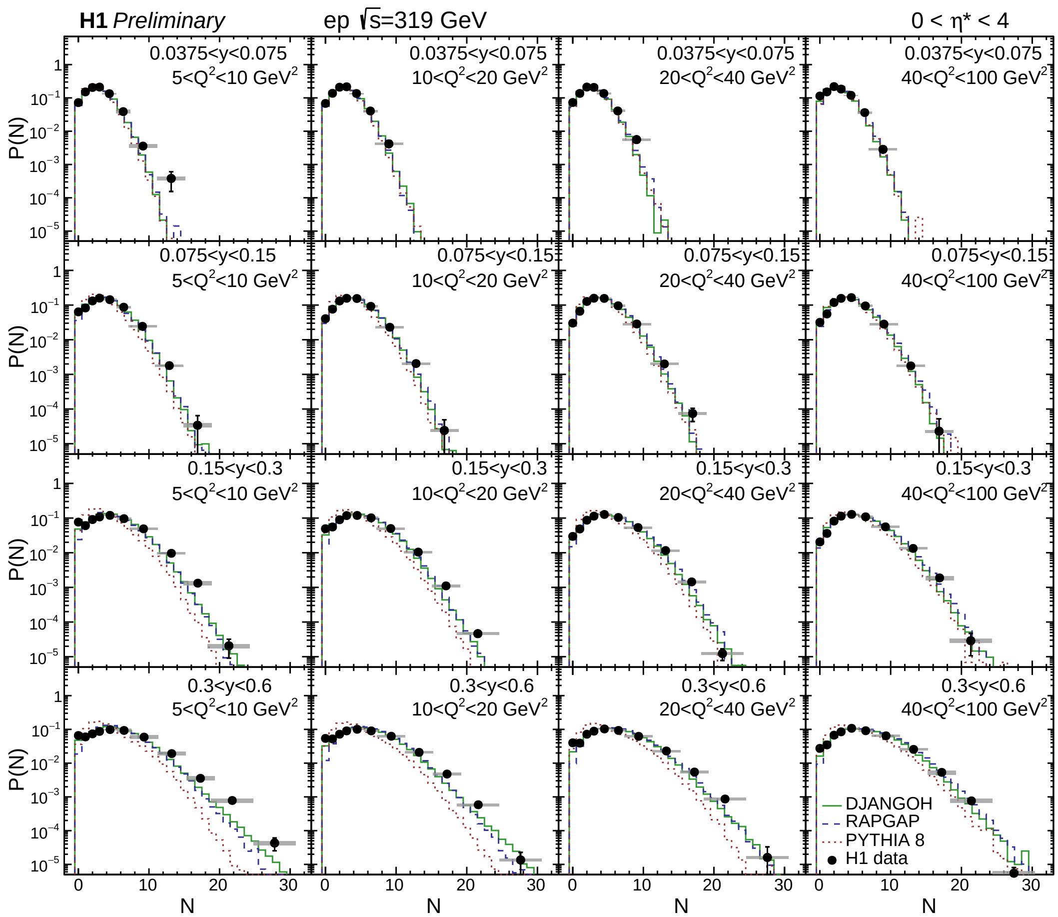

Figure 6: The charged particle multiplicity distributions, $P(N)$, are shown as a function of N particles at $\sqrt{s} = 319\,\mathrm{GeV}$ ep collisions for particles produced within pseudorapidity range $0 < \eta^* < 4.0$ in the HCM frame. Different panels correspond to different Q^2 and y bins, indicated by the legends in the figure. The MC particle level multiplicity distributions from DJANGOH, RAPGAP, and PYTHIA 8, are also shown for comparison. The statistical uncertainty is denoted by the error bars. The systematic uncertainty is shown with the shaded box. For intervals wider than one unit in multiplicity, the quantity $P(N)/\Delta N$ is shown. Along the horizontal axis, the data are drawn at the geometrical bin center.

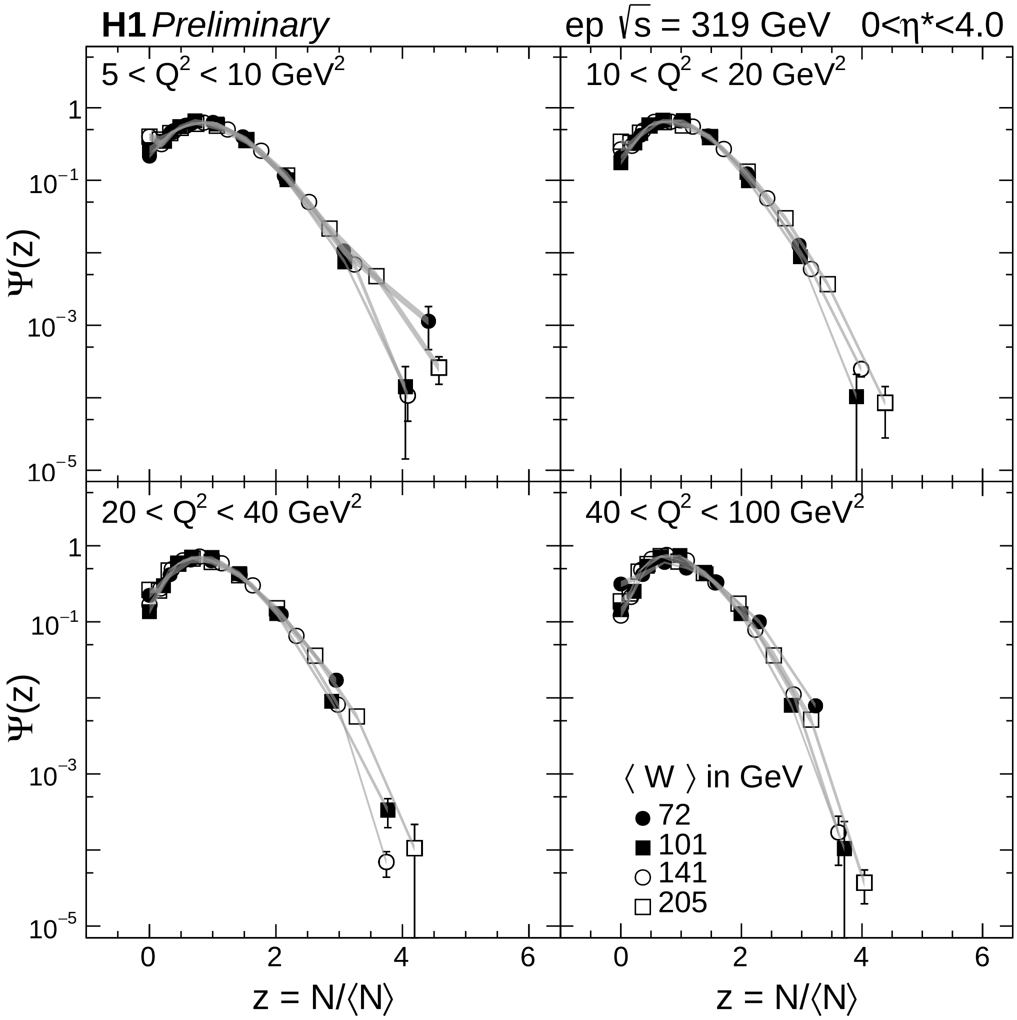

Figure 7: The KNO function, $\Psi(z)$, are shown as a function of z at $\sqrt{s} = 319\,\mathrm{GeV}$ in ep collisions for particles with transverse momentum $p_{\mathrm{T,lab}} > 150\ \mathrm{MeV/c}$ produced within pseudorapidity range $0 < \eta^* < 4.0$ in the HCM frame. Different panels correspond to different Q^2 bins, where different y (or $\langle W \rangle$) bins indicated by the legends in the figure. The statistical uncertainty is denoted by the error bars. The systematic uncertainty is shown with the shaded band.

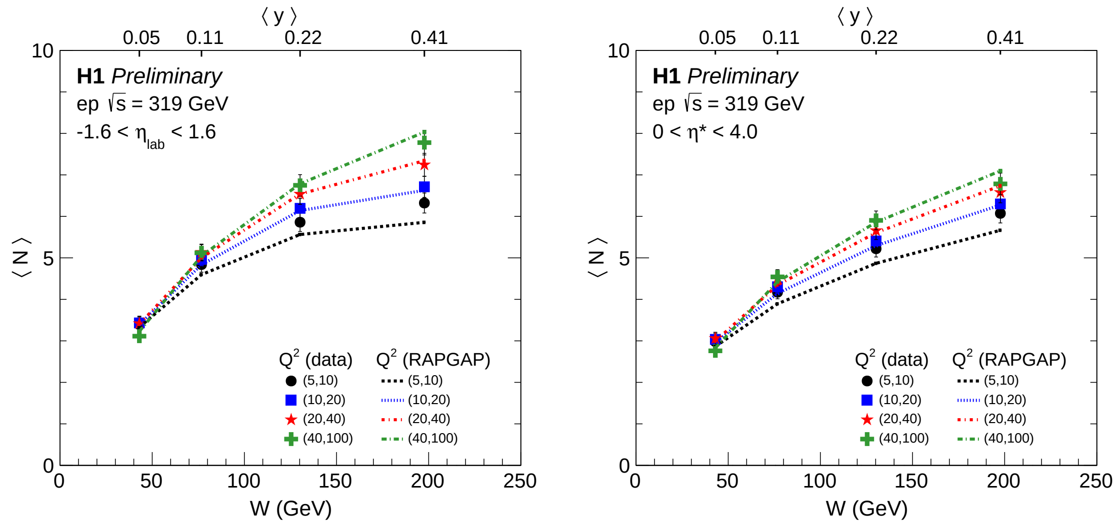

Figure 8: The mean multiplicity, $\langle N_{\rm ch}\rangle$, is shown as a function of W at $\sqrt{s} = 319\,\mathrm{GeV}$ ep collisions for particles with transverse momentum $p_{\rm T,lab} > 150\ \mathrm{MeV/c}$ within pseudorapidity range $|\eta_{\rm lab}| < 1.6$ in the lab frame (left) and $0 < \eta^* < 4.0$ in the HCM frame (right). The $\langle y\rangle$ is also indicated by the top axis for each measured bin. The MC models are denoted by dashed lines. The total uncertainty is represented by the error bar.

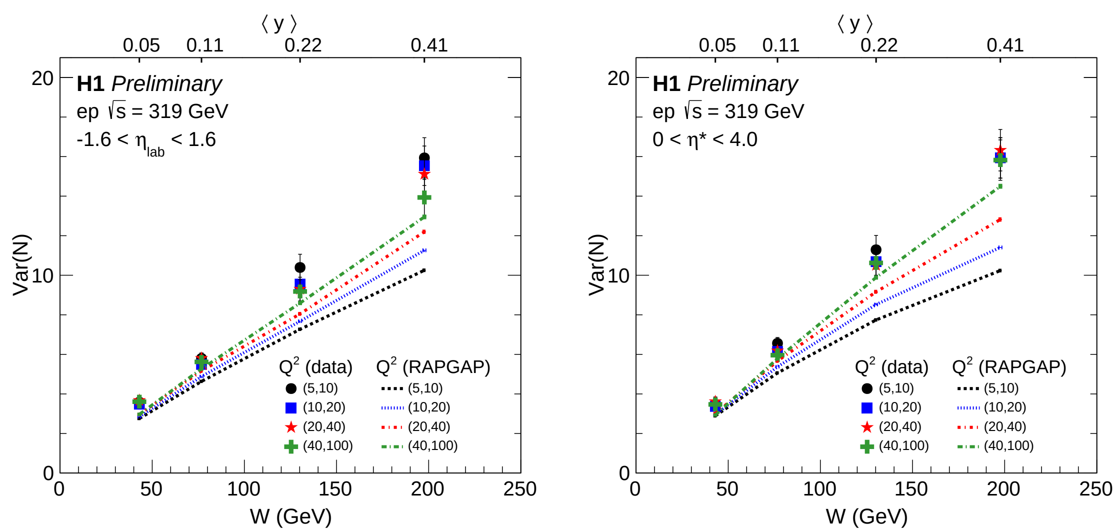

Figure 9: The second moment, variance, is shown as a function of W at $\sqrt{s} = 319\,\mathrm{GeV}$ ep collisions for particles with transverse momentum $p_{\rm T,lab} > 150\ \mathrm{MeV/c}$ within pseudorapidity range $|\eta_{\rm lab}| < 1.6$ in the lab frame (left) and $0 < \eta^* < 4.0$ in the HCM frame (right). The $\langle y\rangle$ is also indicated by the top axis. The statistical uncertainty is denoted by the error bar.

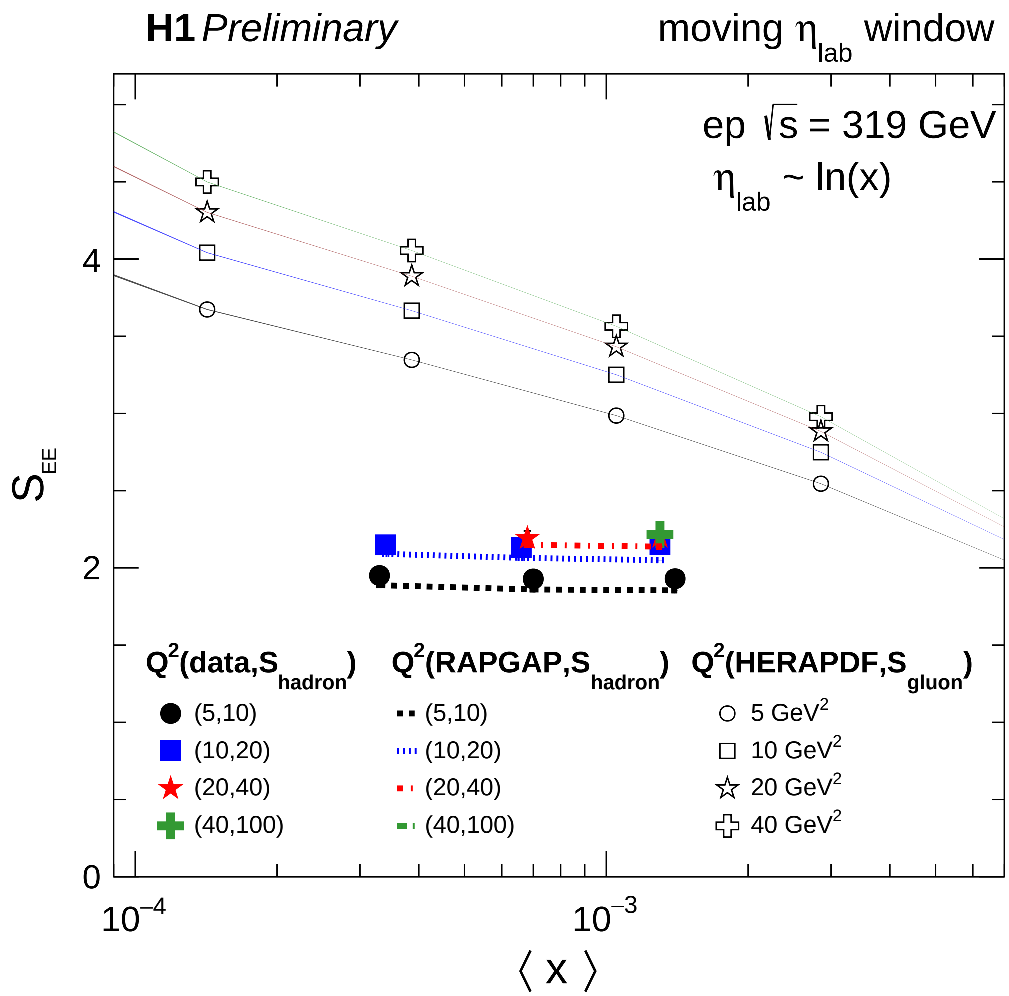

Figure 10: The Boltzmann entropy based on the multiplicity distributions, is shown as a function of $\langle x \rangle$ at $\sqrt{s} = 319\,\mathrm{GeV}$ ep collisions for particles with transverse momentum $p_{\mathrm{T,lab}} > 150\ \mathrm{MeV/c}$ within pseudorapidity ranges $-1.2 < \eta_{\mathrm{lab}} < 0.2$ ($\langle x \rangle \sim 3 \times 10^{-4}$), $-0.5 < \eta_{\mathrm{lab}} < 0.9$ ($\langle x \rangle \sim 7 \times 10^{-4}$), and $-0.2 < \eta_{\mathrm{lab}} < 1.6$ ($\langle x \rangle \sim 1.3 \times 10^{-3}$) in the lab frame with different Q^2 ranges. The MC models are denoted by dashed lines. The total uncertainty is represented by the error bar. The theoretical predictions of entanglement entropy based on the gluon density $xG(x)$ are also presented at different Q^2 indicated by the legends. The PDF set is HERAPDF 2.0 at the leading order.

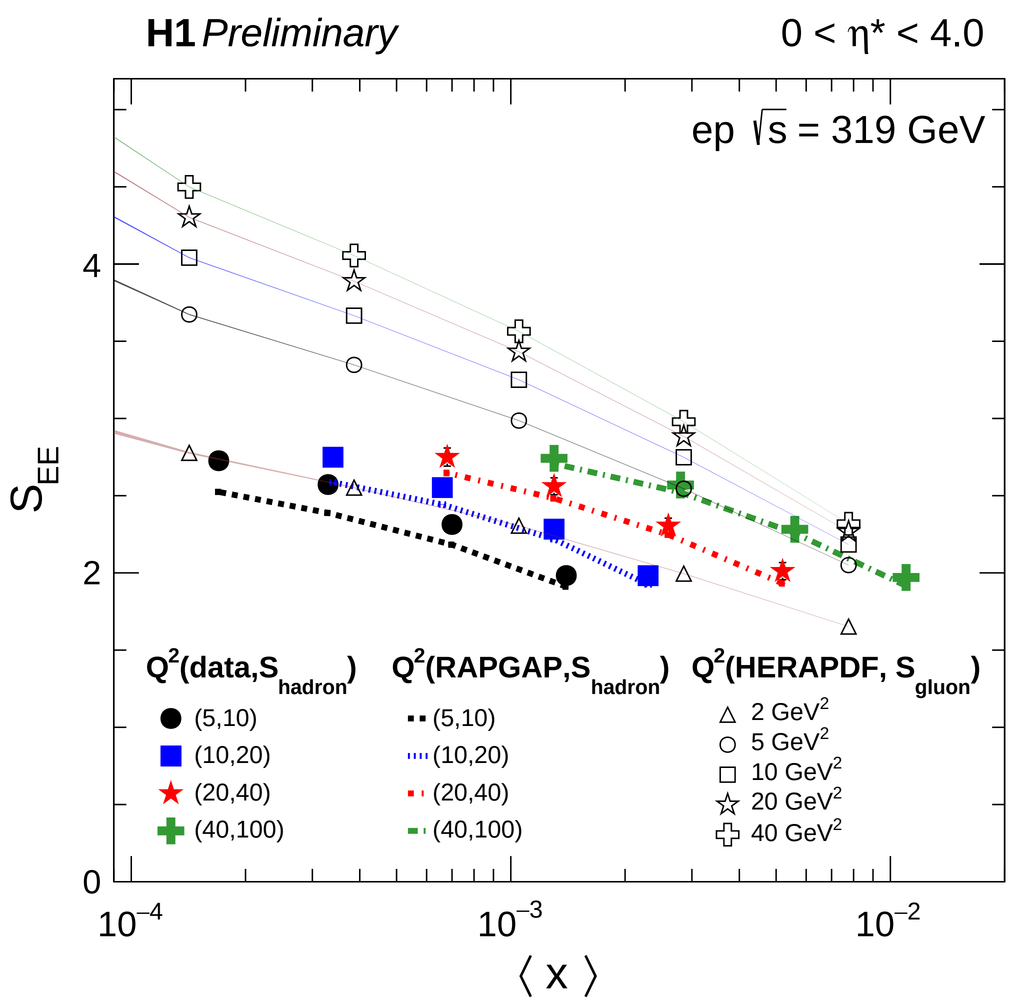

Figure 11: The Boltzmann entropy based on the multiplicity distributions, is shown as a function of $\langle x \rangle$ at $\sqrt{s} = 319\,\mathrm{GeV}$ ep collisions for particles with transverse momentum $p_{\mathrm{T,lab}} > 150\,\mathrm{MeV/c}$ within pseudorapidity range $0 < \eta^* < 4.0$ in the HCM frame with different Q^2 ranges. The MC models are denoted by dashed lines. The total uncertainty is represented by the error bar. The theoretical predictions of entanglement entropy based on the gluon density $xG(x)$ are also presented at different Q^2 indicated by the legends. The PDF set is HERAPDF 2.0 at the leading order.